Supporting Information for

Modulating and self-assembly of nanoparticles into bismuth molybdate nanosheets as high-efficient photocatalyst for ciprofloxacin degradation

Juan Zhang,[a] Yating Wang,[a] Yuan Wang,[a] Xiaofeng Shuai,[a] Ruihua Zhao,[b,*] Umsalama Abuelgasim Abubakr Yasin,[a] Tianyu Guo,[c] Jianping Du, [a,d,*] Jinping Li [a,d]

[a]College of Chemistry, College of Chemical Engineering and Technology, Taiyuan University of Technology, 79 Yingze West Street, Taiyuan 030024, Shanxi, PR China. E-mail: dujp518@163.com

[b]Shanxi Kunming Tobacco Co. Ltd., 21 Dachang South Road, Taiyuan 030032, Shanxi PR China. E-mail: zhrh6688@163.com

[c] College of Environment Science and Engineering, Taiyuan University of Technology, No.209 University Street, Jinzhong 030600, Shanxi, PR China

[d]Shanxi Key Laboratory of Gas Energy Efficient and Clean Utilization, No.79 West Street, Taiyuan 030024, Shanxi, PR China

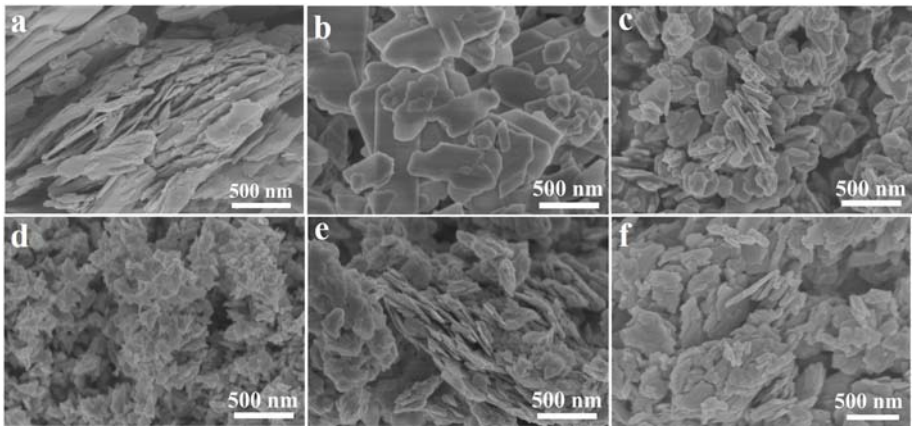

Figure S1 SEM images of as-obtained (a) BMO-PEG (b) BMO-EDTA, (c) BMO-TA, (d) BMO-Sorb, (e) BMO-CA-0.2, (f) BMO-CA-0.4

The role of additives and explanations:

The morphology and structures of as-prepared Bi_2MoO_6 materials have been affected by the amount and types of surfactants, and the growth mechanisms are different in the synthesis system, which are dependent on their molecular structure and intrinsic characteristics. Polyethylene glycol (PEG) is a non-ionic surfactant and has long chain of alkyl zigzag molecules with alcohol hydroxyl groups at both ends. EDTA is an useful chelate. Sorbitol (sorbic alcohol) belongs to alcohol, and tartaric acid and citric acid are organic acid. From molecule level, these substances have different molecular structures that play a distinct role in synthetic reaction of Bi_2MoO_6. In the process of PEG-assisted growth, the micellar particles formed with bismuth and molybdate ions grow along the micelle direction, but depress the formation of larger sheet structures. High specific surface energy of small size causes spontaneous aggregate of nanosheets. Chelation effect of EDTA controls concentrations of ions, which can effectively regulate the growth rate and size of nanosheets. Sorbitol is a polyhydroxy compound and can combine easily with bismuth ion. The resulting molybdate precursor by electrostatic attraction was pyrolyzed to produce fragments that are grown to small nanosheets and the stacking structures are formed due to agglomeration. In the present of tartaric acid, it controls the nucleation and growth of Bi_2MoO_6, thus the resulting complex compound remains lamellar molecule structure and lead to formation of small nanosheets. For comparison, citric acid has more carboxyl groups and it can form hydrogen bond between carboxyl and hydroxyl groups and form complex with bismuth ion, thus leading to formation of chelate with molybdate by electrostatic effect. In the process of pyrolysis, small-size and well-dispersed nanoparticles are produced easily and self-assembly of monolayer nanoparticles into nanosheets were achieved by citric acid molecule obstructing. With increasing citric acid concentration, the size of nanosheets trend to decrease. Thus high surface energy of nanoplates lead to aggregate and the stacked structure are formed. Therefore, high dispersed nanosheets that are composed of nanoaparticles possess high reactive surface and provide more active sites for photocatalytic reaction.

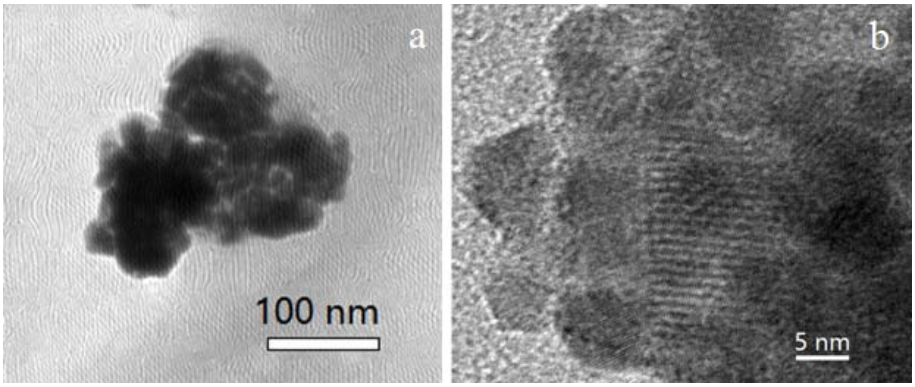

Figure S2 Magnified typical TEM images of BMO-CA-0.3 nanoparticles. It shows that some aggregates (black dots shown in low resolution image) are composed of nanoparticles.

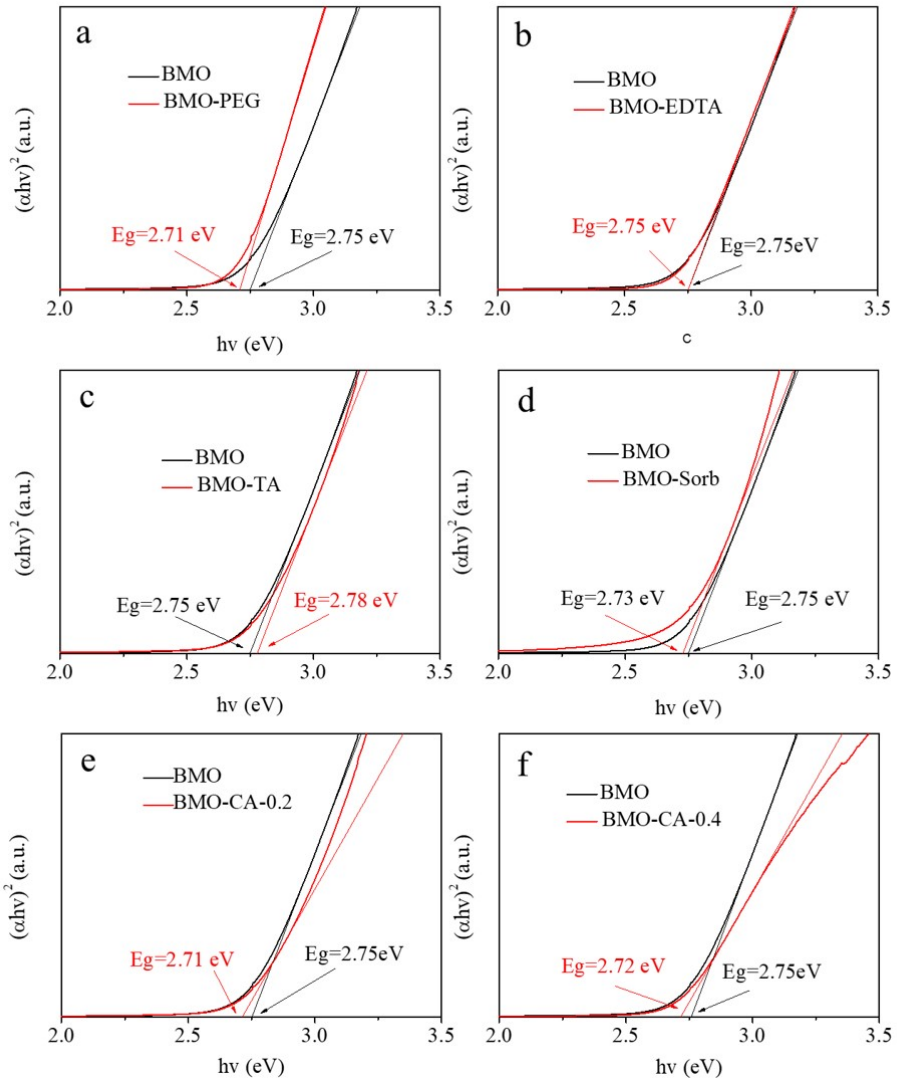

Figure S3 The band gaps of (a) BMO-PEG, (b) BMO-EDTA, (c) BMO-TA (d) BMO-Sorb, (e) BMO-CA-0.2 (f) BMO-CA-0.4

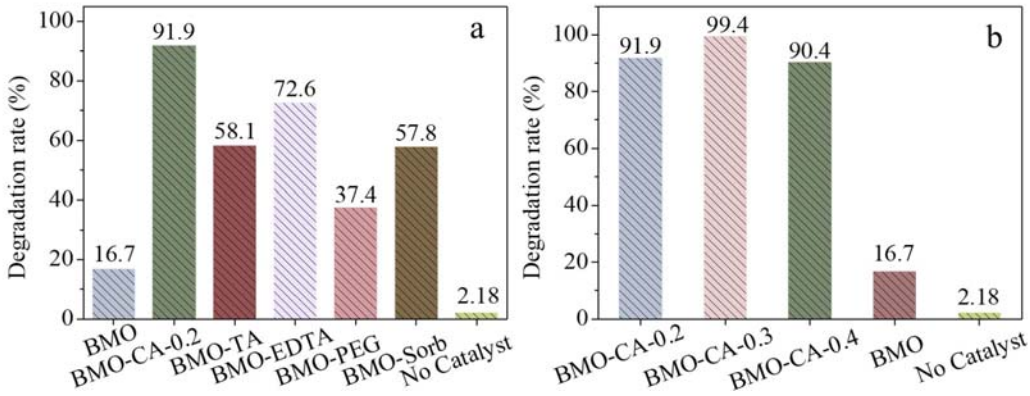

Figure S4 Photodegradation rates of CIP over different photocatalysts (a) and BMO-CA (b) after 120 min under visible light.

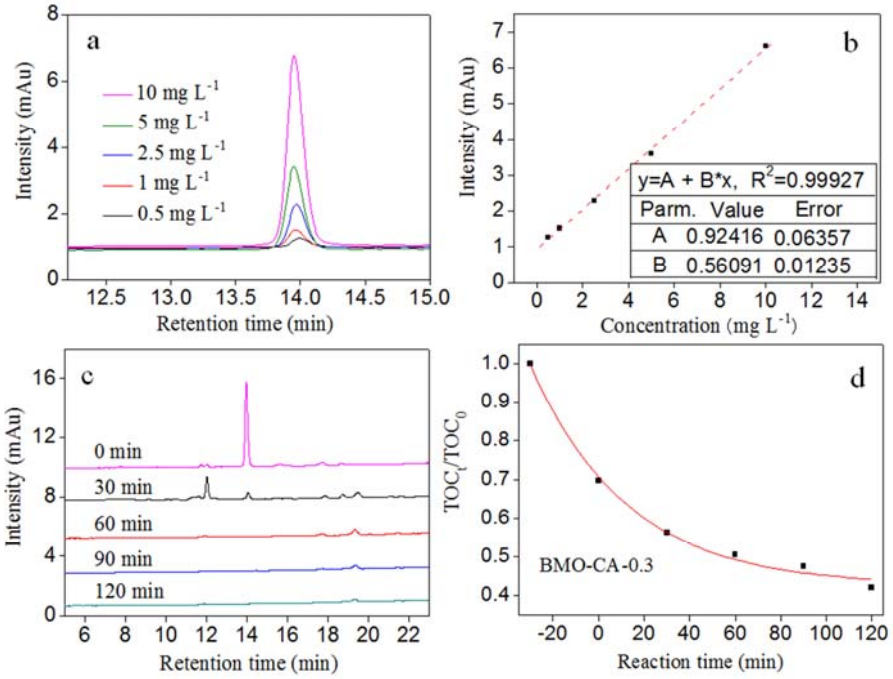

Figure S5 (a) Typical HPLC chromatograms of CIP (0.5, 1.0, 2.5 5.0 and 10.0 mg L^{-1}, respectively), (b) the corresponding calibration curve (the linear coefficient (R^2) was 0.99927), (c) HPLC chromatograms of CIP degraded for different times (0, 30, 60, 90 and 120 min, respectively) and (d) The TOC values of CIP solution after the degradation of different time over the BMO-CA-0.3 material

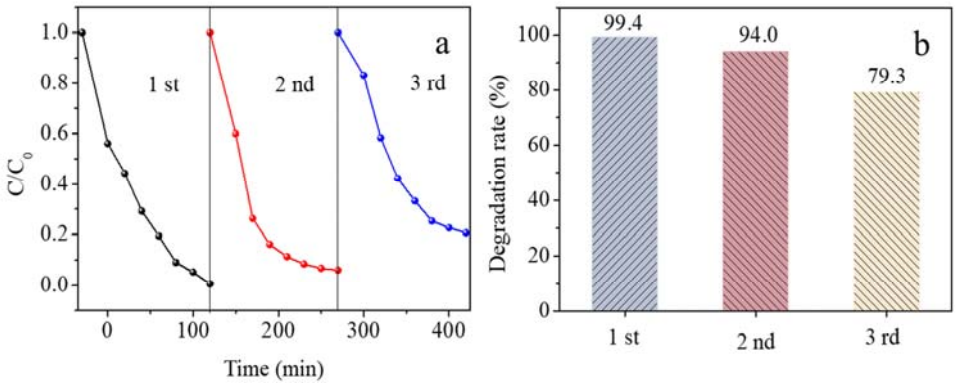

Figure S6 (a) The photocatalytic degradation of CIP over BMO-CA-0.3 running three-cycle tests and (b) Photodegradation rates of CIP over BMO-CA after 120 min

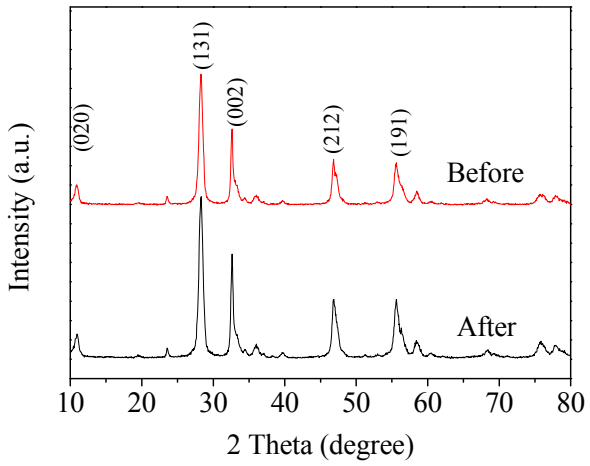

Figure S7 XRD of the BMO-CA-0.3 photocatalyst before and after the degradation reaction

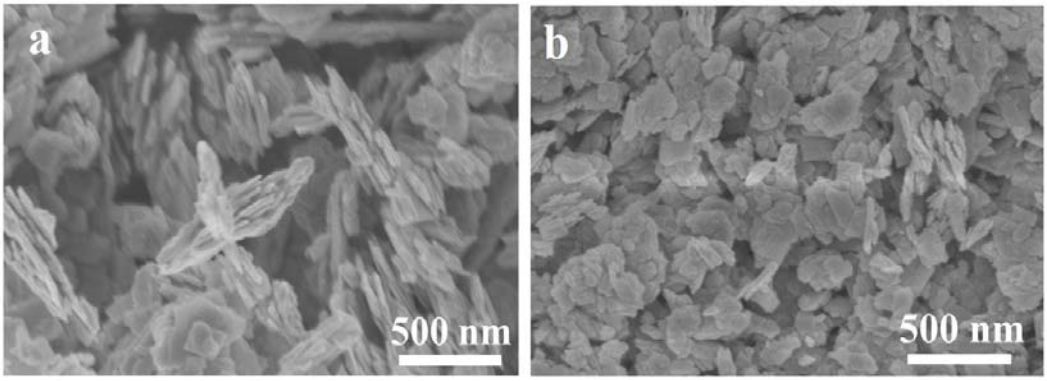

Figure S8 SEM images of the BMO-CA-0.3 (a) before and (b) after the degradation reaction

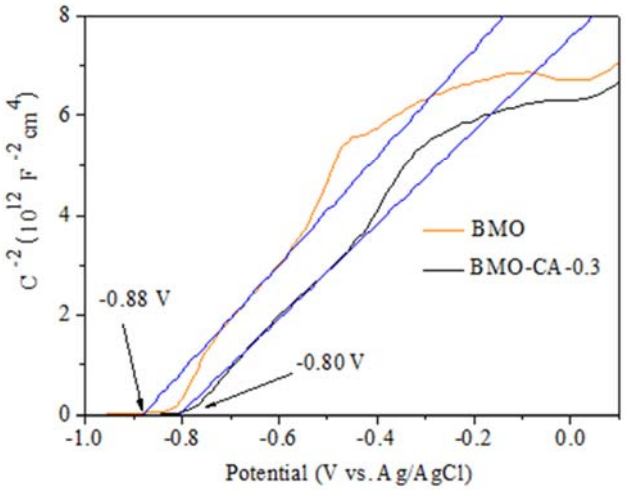

Figure S9 Mott-Schottky plots of BMO and BMO-CA-0.3 materials

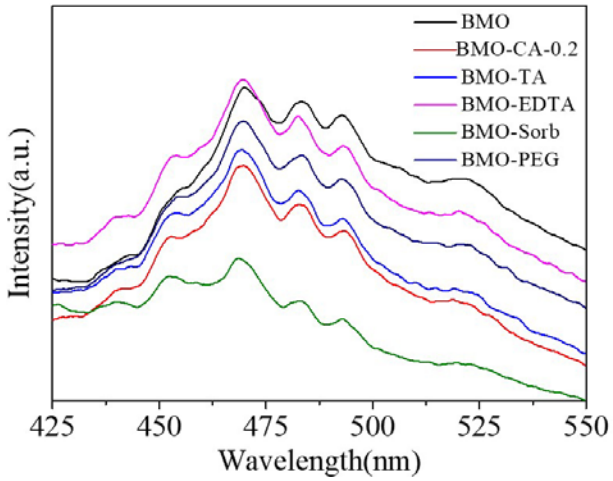

Figure S10 PL spectra of BMO and BMO prepared with different surfactants-assisted strategy

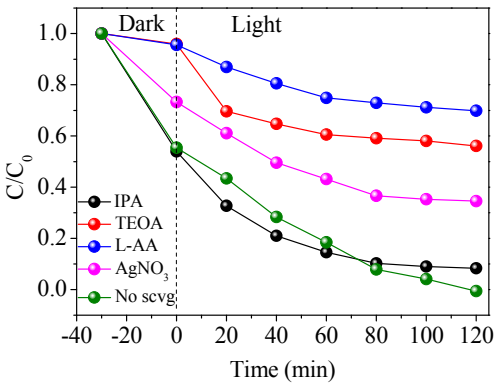

Figure S11 CIP degradation rate over BMO-CA-0.3 in the presence of different radical scavengers under visible light for 120 min

Table S1 Comparison of as-prepared Bi_2MoO_6 nanosheets (BMO) with some reported materials

Catalysts	Dosage (mg)	Light source (W)	CIP Conc./ Volume (mg L^{-1}/mL)	Irradiation time/ Degrade. Efficiency (min/%)	Ref.
Bi_2MoO_6/ RGO	50	300W[b]	20/50	360/90	[1]
CdS /RGO/Bi_2MoO_6	200	500W[a]	20/40	60/91	[2]
CQD/Bi_2MoO_6	50	300W[a]	10/100	120/88	[3]
WS_2/ Bi_2MoO_6	250	500W[a]	10/250	180/98.9	[4]
Ag/$Ag_6Si_2O_7$/Bi_2MoO_6	50	300W[a]	20/100	120/96.63	[5]
Bi_2MoO_6/ SnS_2	N.A.	5W[c]	10/50	120/90	[6]
BiOBr/ Bi_2MoO_6	50	300W[a]	10/50	120/84.63	[7]
Bi_2MoO_6/$CuBi_2O_4$	200	500W[a]	10/200	180/90.2	[8]
Bi_2MoO_6/g-C_3N_4	50	N.A.	10/100	120/76.5	[9]
BMO	50	300W[a]	10/100	120/99.4	This work

a. Xe lamp (λ>420nm), b. halogen lamp, c. LED light, d. an 8-tube photoreaction system.

References

[1] J. Bai, Y. Li, X. Li, L. Liu, New J Chem 2017, 41, 7783-7790.

[2] Z. Chen, J. Liang, X. Xu, G. He, H. Chen, J. Mater. Sci.2020, 55, 6065-6077.

[3] J. Di, J. Xia, M. Ji, H. Li, H. Xu, H. Li, R. Chen, Nanoscale, 2015, 7, 11433-11443.

[4] X. Li, M. Su, G. Zhu, K. Zhang, X. Zhang, J. Fan, Dalton Trans, 2018, 47, 10046-10056.

[5] S. Li, B. Xue, J. Chen, Y. Liu, J. Zhang, H. Wang, J. Liu, Sep. Purif. Technol. 2021, 254,117579.

[6] H. Liu, C. Du, H. Bai, Y. Su, D. Wei, Y. Wang, G. Liu, L. Yang, J. Mater. Sci. 2018, 53, 10743-10757.

[7] S. Wang, X. Yang, X. Zhang, X. Ding, Z. Yang, Appl. Surf. Sci. 2017, 391, 194-201.

[8] Z Li, R Zheng, S Dai, T Zhao, M Chen, Q Zhang, J. Alloys Compd. 2021, 882, 160681.

[9] B. Li, C. Lai, L. Qin, C. Chu, M. Zhang, S. Liu, X. Liu, H. Yi, J. He, L. Li, M. Li, L. Chen, J Colloid Interface Sci 2020, 560, 701-713.